The 8th European Congress on Computational Methods in Applied Sciences and Engineering
ECCOMAS Congress 2022
5 – 9 June 2022, Oslo, Norway

SIMULATION AND EXPERIMENTAL INVESTIGATION OF TIRE TREAD BLOCK WEAR IN THREE-BODY CONTACT

Duc Nam Nguyen[1] and Stephanie Kahms[2]

[1] Leibniz University Hannover, Institute of Dynamics and Vibration Research, An der Universität 1, 30823 Garbsen, nguyen.duc@ids.uni-hannover.de, www.ids.uni-hannover.

[2] Leibniz University Hannover, Institute of Dynamics and Vibration Research, An der Universität 1, 30823 Garbsen, kahms@ids.uni-hannover.de, www.ids.uni-hannover.de

Key words: three-body contact, abrasive wear, tire modeling, particles.

Abstract. *On gravel roads, tires are not in direct contact with the surface. Particles of e.g. sand or stone contact directly with the tire and cause the tire to wear. During the sliding process, an interaction between particles and the tire occurs. On simplified conditions investigation of the movement of particles, friction and wear of a tire tread sample are done experimentally for different settings. Additionally, a finite element simulation is built up to simulate the wear of the tire tread sample under varying conditions. In this paper results from the experimental and numerical investigation of the wear of the tire tread sample are shown.*

I INTRODUCTION

In three body contact of a tire, particles and road surface, particles form an intermediate layer between the tire and the road surface. The particles either are embedded in the tire surfaces or are free to roll and slide [1]. Moving particles cause the tire to wear [2]. The abrasive wear process on three-body abrasion depends on many parameters as contact pressure, velocity, material, abrasive particle properties, and surface roughness. The influence of these factors contributes to complex contact conditions resulting in different wear mechanisms of the tires.

In general, experimental and numerical methods are chosen to predict the wear rate of tires. An experimental approach is often proposed to investigate the wear behavior, such as the determination of mass loss, wear rate, and examination of the worn surface. The experimental method is efficient and often useful because all physical effects and their interactions are combined. However, experiments are expensive, time-consuming, and are only valid for the used test configurations. Numerical simulations are used to investigate the relevant factors of abrasion. The simulation results also provide further information during the wear process, such as changes in the worn surface and pressure, in order to better understand the wear behavior [3,4].

The paper focuses on the mechanical modeling and abrasive wear simulation of the tire tread sample in three-body contact (tire tread sample, particles, and road). The model is constructed two-dimensionally (2D) for consideration of the high demand for computing power. The finite element method is chosen to describe the dynamical behavior of the tire tread sample. The model can simulate the tire tread sample's time-dependent wear depth, wear rate, and local contact pressure. The influence of parameters, such as contact pressure, velocity, sliding distance, and material properties on the wear behavior, is considered in the simulation. The results of the wear simulation are compared to the experimental results. Similarities and differences between the simulation and experimental wear results are analyzed and compared to indicate the model's usefulness and limitations.

2 STRUCTURE OF THE SIMULATION MODEL

2.1 Geometric and material model of tire tread sample

The wear simulation is based on a tire tread block that is fixed on a steel plate. The road surface carries the particles and is modeled as a mobile object. This means that effects arising from the dynamics of the remaining tire and the rest of the vehicle are neglected. The model is constructed two-dimensionally for considering of high demand for computing power. The model's basic structure with translational motion is shown in Figure 1.

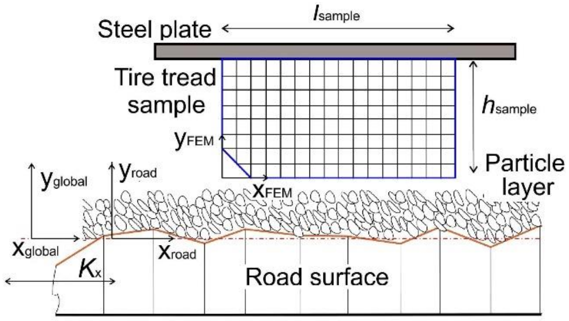

Figure 1. Structural dynamic model

The finite element method is applied to depict the dynamical behavior of the tire sample. The sample is modeled as a rectangle with homogeneous density and stiffness distribution in the unstressed state. The sample is also chamfered so that the abrasive particles can enter the contact area more easily. The dimension of the tire sample is 20mm in length, 10mm in height, and 2mm in chamfer.

The tire tread sample is modeled as a linear system. The particular material properties of the rubber, e.g. the Mullins effect and Payne effect, are neglected and not included in the model. The tire sample is meshed in two-dimensional geometry. It is suitable to cross-link the rectangular sample with quadrilateral elements. The length of the elements is approximately 1mm. The origin of the coordinate system is in the lower-left corner of the sample, as shown in Figure 2. The contact nodes located on the underside are all located on the *x*-axis.

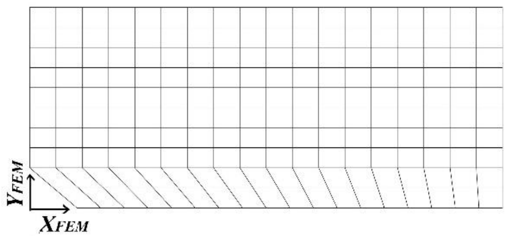

Figure 2. Coordinate and mesh of the tire tread sample

The principle of virtual work is applied to obtain the element mass matrix and the element stiffness matrix for the quadrilateral elements [5,6].

The mass matrix for an element can be written as

$$[M] = \iint \varrho [N]^T [N] t dx dy = \int_{-1}^{1} \int_{-1}^{1} \varrho [N]^T [N] t J d\xi d\eta . \tag{1}$$

The density ϱ of the rubber material has been determined by weighing a defined rubber volume to $\varrho = 1.16 \cdot 10^{-3}$ (g/mm^3)

The stiffness matrix for an element can be written as

$$[K] = \iint [B]^T [E'] [B] t dx dy = \int_{-1}^{1} \int_{-1}^{1} [B]^T [E'] [B] t J d\xi d\eta . \tag{2}$$

For the case of two-dimensional plane stress analysis, the material constitutive matrix [C] is

$$[C] = \frac{E'}{(1-\nu^2)}\begin{bmatrix} 1 & \nu & 0 \\ \nu & 1 & 0 \\ 0 & 0 & \frac{(1-\nu)}{2} \end{bmatrix}. \tag{3}$$

Where E' is the dynamic elastic modulus or storage modulus and ν is the Poisson's ratio. The Poisson's ratio ν is set to the value of $\nu = 0.49$, which is characteristic for the nearly incompressible material. The dynamic elastic modulus E' and the loss modulus E'' are measured experimentally by performing Dynamical Mechanical Analysis (DMA) at German institute for rubber technology (DIK), shown in Figure 3.

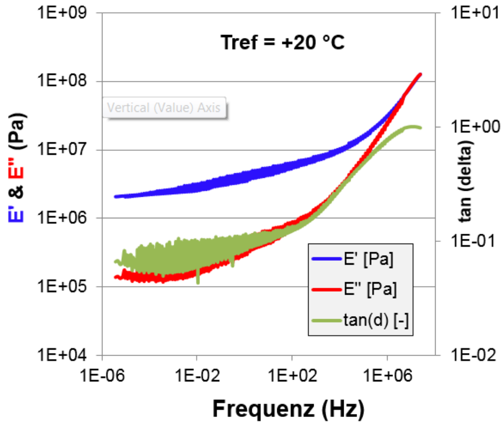

Figure 3. The experimental data of the dynamic elastic modulus E' and the loss modulus E''

To fit the experimental data of the dynamic elastic modulus E', the Prony series [7] is very suitable. The dynamic elastic modulus E' are represented in Prony series as follows

$$E'(\omega) = E_\infty + \sum_i \frac{E_i \omega^2 \tau_i^2}{1+\omega^2\tau_i^2}, \tag{4}$$

$$E'(t) = E_\infty + \sum_i E_i e^{\frac{-t}{\tau_i}}. \tag{5}$$

The dynamic elastic modulus E' is represented as functions of frequencies in equation (4) and time in equation (5). In this work, 19 Maxwell branches (s. table 1) are used to determine to fit the experimental data. Figure 4a and Figure 4b show the plots of E' as approximate functions of frequencies and time.

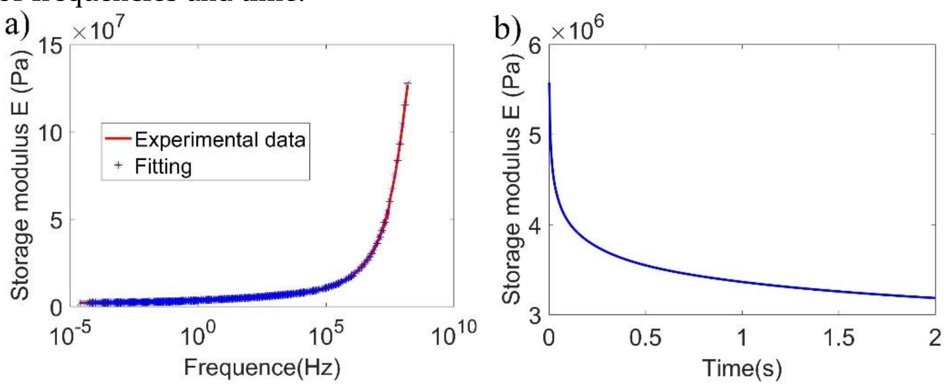

Figure 4. The fitting curve of the dynamic elastic modulus E' depending on frequency (a) and time (b)

Table 1: The Prony parameters for fitting the dynamic elastic modulus E'

Index i	E_i	τ_i
∞	2.066e+06	-
1	4.077e+04	41819,8628
2	9.067e+04	8844,4037
3	1.899e+05	1870,4862
4	1.244e+05	395,5855
5	1.834e+05	83,6616
6	2.354e+05	17,6934
7	4.250e+05	3,7419
8	4.264e+05	0,7913
9	5.103e+05	0,1673
10	5.593e+05	0,0353
11	6.869e+05	0,748e-02
12	8.405e+05	0,158e-02
13	1.007e+06	0,334e-03
14	1.261e+06	7,081e-05
15	2.391e+06	1,497e-05
16	3.879e+06	3,167e-06
17	8.127e+06	6,698e-07
18	1.4162e+07	1,416e-07
19	4.187e+07	2,995e-08

The equivalent damping matrix D is modeled as proportional to the stiffness matrix K, based on the widely propagated Rayleigh damping in the structural dynamics [8]

$$D = \beta K . \tag{6}$$

The stiffness damping parameter β is determined by the following relationship [8]

$$\beta = \eta/2\pi f = \eta/\omega . \tag{7}$$

The loss factor η is calculated according to the following relationship

$$\eta = E''/E' . \tag{8}$$

In the sliding process, the tire tread sample is worn out and causes the shape of the sample to change over time. In addition, the dynamic elastic modulus E' also changes over time. Therefore the element mass matrix M and the element stiffness matrix M are recomputed with the change of tire sample's geometry and the dynamic elastic modulus E' after each wear simulation time step.

The structural dynamics problem is based on the following basic equation:

$$M\ddot{\vec{q}} + D\dot{\vec{q}} + Kq = \vec{F} = \vec{F_x} + \vec{F_y} . \tag{9}$$

The inputs are the forces at contact nodes, the mass matrix *M*, the stiffness matrix *K*, and the damping matrix *D*. The outputs are the node positions and the node velocities. These output parameters then are used in "wear model" that is described in section 2.3 in more detail.

2.2 Road and Particle layer model

The tire tread sample described above is considered as the first contact partner of three-body contact. Next, the particles and the road surface are implemented as second and third contact partners in the simulation model.
During three-body contact, the particles act as an intermediate layer separating the contact between the road surface and the rubber sample. The tire tread sample will directly contact the particles and causes the wear of the tire tread sample. There is a significant difference in the hardness of the particles and the tire tread sample. While the particles have a high modulus of elasticity, the rubber compound of the tread is comparstively soft. In addition, the particles are also renewed after each experiment. It can therefore be assumed that the particles do not wear out and do not break during contact. In wear simulation, the particles between two contacting surfaces are described as a solid layer represented by nonlinear springs, shown in Figure 5.

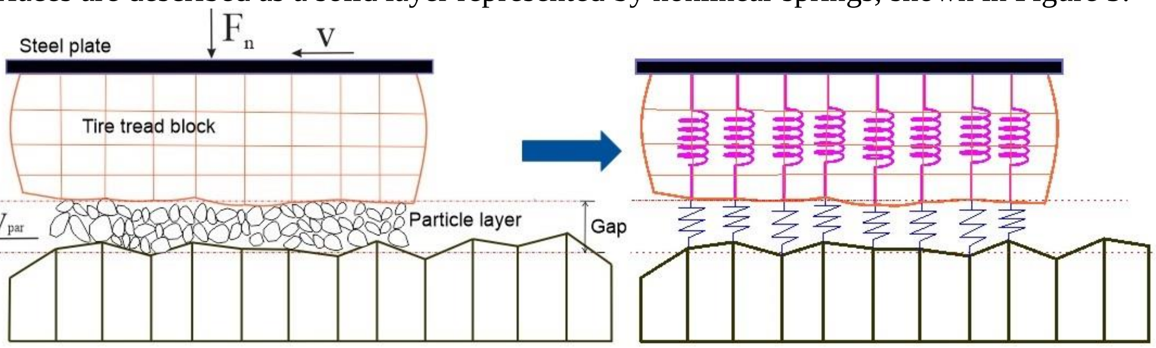

Figure 5. The particles are assumed as a solid layer represented by nonlinear springs

The particles also contact with the road surface and cause wear to the road surface. However, in the experimental process, the sandpaper is used as road surface and replaced frequently, so the sandpaper wear is also insignificant. Therefore, the material properties of the road surface are ignored and only the topography of the surface is considered. The waviness and roughness of the sandpaper surface were measured using an Alicona microscope. In this study, in order to reduce simulation time, waviness is applied to represent the road surface profile. The experimental waviness of the road surface is fitted by a superposition of several sine waves. Figure 6 shows the experimental and fitting surface of sandpaper P120.

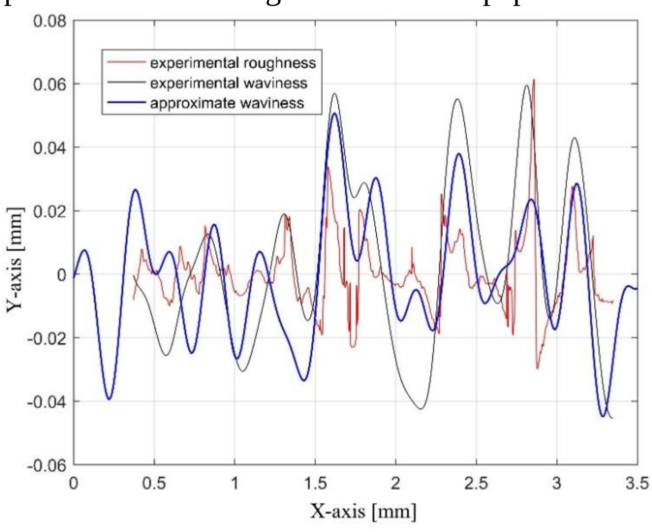

Figure 6. The experimental and approximate surface profile of sandpaper 120

2.3 Wear model

The Wear is a consenquence of friction between contact bodies. In this work, the wear model is described according to [9,10]. In this wear model, the wear volume

$$V = k_a \mu p_n^{k_p} v^{k_v} SL \tag{10}$$

is a result of friction coefficient μ, normal pressure p_n, sliding velocity of sample v, sliding distance SL, and wear coefficient k_a, k_p, and k_v.
From the wear volume, the height reduction at each contact node of the tire tread sample is defined as follows

$$l_{w,i} = \int \frac{1}{\varrho A_i n_{no}} k_a v_{rel,i} \mu\, p_{n,i}^{k_p} v_{rel,i}^{k_v} dt\ , \tag{11}$$

where A_i is the mean of the area assigned to the local contact element i, n_{no} is number of the contact nodes, $p_{n,i}$ is the normal pressure

$$p_{n,i} = \frac{F_{n,i}}{A_i}\ , \tag{12}$$

$$F_{n,i} = C_R.\left(y_{road} + y_{par} - q_{y,i} - Gap\right)\ , \tag{13}$$

and $v_{rel,i}$ is the relative velocity between the tire tread sample and particle layer of contact node i

$$v_{rel,i} = v - v_{par} - \dot{q}_{x,i}\ . \tag{14}$$

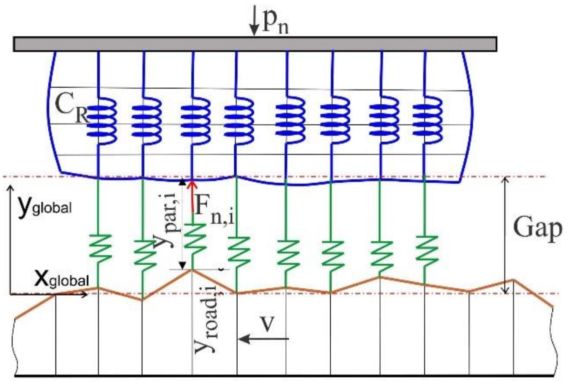

Figure 7. The coordinate in *y*-direction of contact node *i* with road surface

In equations (12) and (14), $\dot{q}_{x,i}$ and $q_{y,i}$ are the velocity in direction x and position in direction y of contact node i. Besides, the remaining parameters such as particle velocity in the contact area v_{par}, contact stiffness of tire tread sample C_R, and the gap between the sample and road surface Gap are determined experimentally.

3 EXPERIMENTAL STUDIES AND RESULTS

The schematic outline of experimental studies is shown in Figure 8. Four experiments, friction and wear measurements of the tire tread sample, investigation of particle displacements, investigation the gap between the tire sample and road surface, and contac stiffness measurement of the tire tread sample, are performed. Then, based on the results of experiments, approximation functions of friction coefficient, velocity, the gap between the sample and road surface, and contact stiffness of tire tread sample dependent on the applied load and the velocity of tire tread are determined. These approximation functions will be used as input parameters in the wear simulation process of the tire tread sample. However, the first two experiments are presented in this paper. These two experiments are performed on the High-speed Linear Tester (HiLiTe), shown in Figure 9.

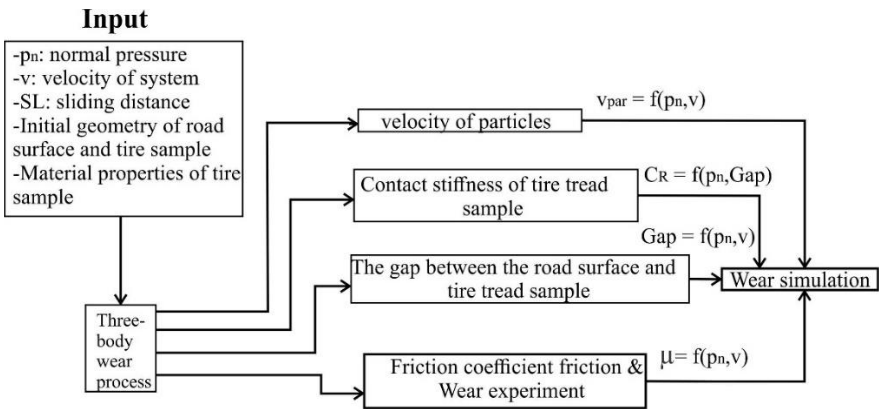

Figure 8. The diagram for experimental studies to define the parameters for wear simulations

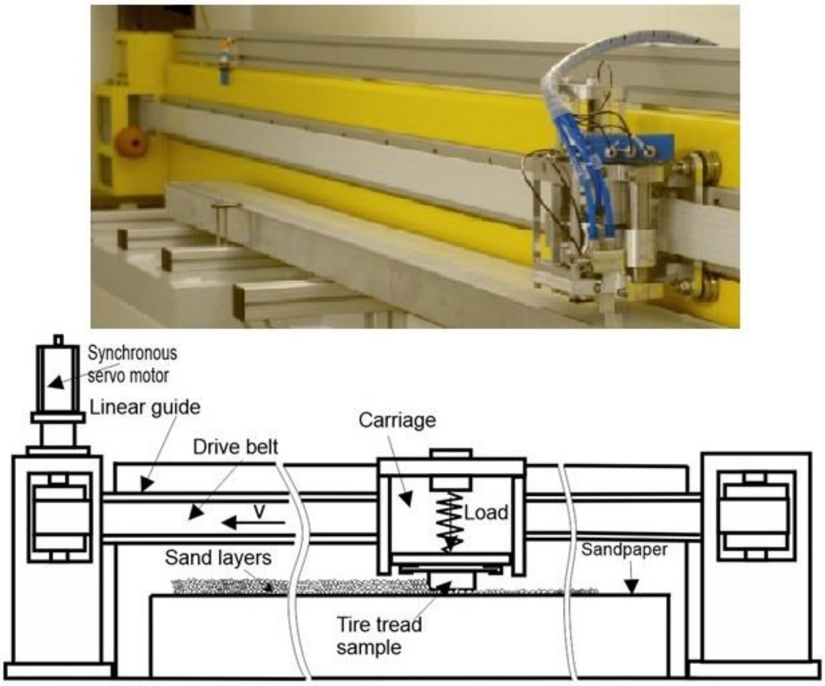

Figure 9. High-speed Linear Tester (HiLiTe)

HiLiTe is one of the test rigs at the Institute of Dynamics and Vibration Research (IDS) at Leibniz University Hannover. HiLiTe enables the experimental investigation of transient friction processes. The principle of the HiLiTe is that the movement between the friction partners is linear and not on a circular. The maximum friction distance is five meters. A servomotor drives, accelerates, and brakes the carriage. The maximum acceleration is 10 m/s^2 and the maximum velocity is 10 m/s. A pre-stressed helical spring is used to generate the normal force in a range between 23 and 1000 N. With a sample size of 20 x 20 mm, normal contact pressures between 0.5 bar and 25 bar can be realized during the test.

Figure 10 describes the schematic diagram of the experiment friction and wear measurement as well as the input and output parameters of the test. This experiment measures the friction coefficient between the tire tread sample and particles, the wear mass of the tire sample as well. The results of this test and approximate curves for experimental data are indicated in Figure 11. Figure 11 a) shows the relation of the friction coefficient with normal pressure and sample velocity. The coefficient of friction increases as normal pressure increases, but the coefficient of friction decreases as sample velocity increases. Figure 11 b) depicts the mass loss variation

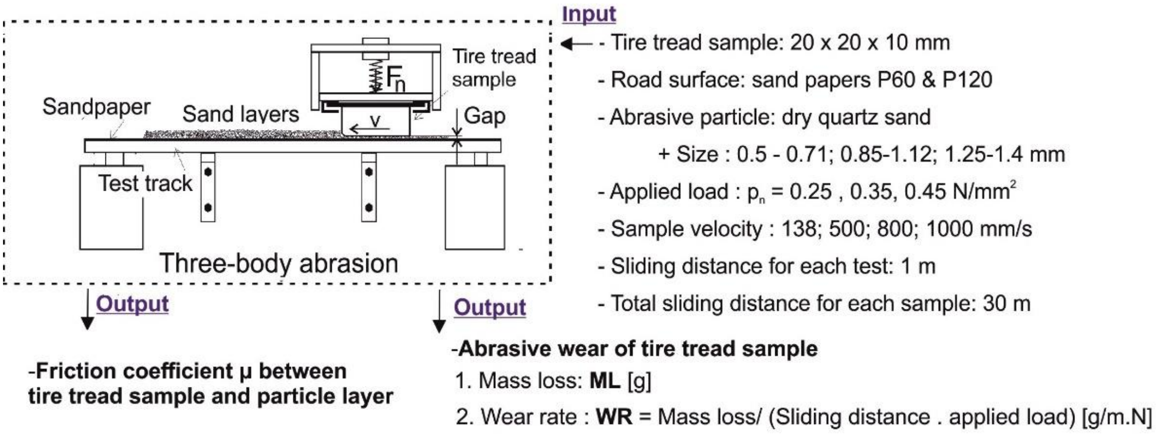

Figure 10. Schematic diagram of the friction and wear measurement

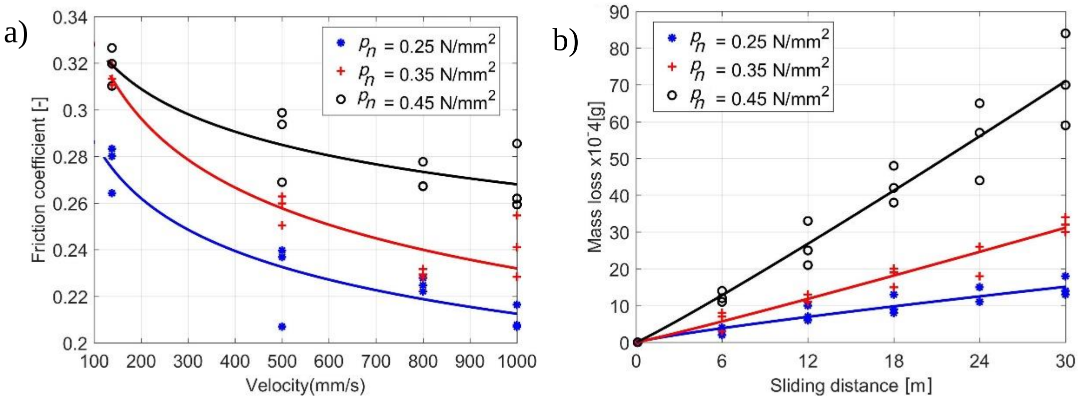

Figure 11. Results and approximiate curves of experiment friction (a) and wear measurement (b)

with the sliding distance change under different applied loads. The mass loss increases with the sliding distance for all normal pressure.

The input, output parameters and the schematic diagram for investigating particle displacements are indicated in Figure 12. Some particles are painted black, the other particles and the road surface are painted white. It is assumed that the velocity of the particles is characterized by the velocity of the black particles. Corresponding to each normal pressure and sample velocity, a total of 20 black sand particles were tested to determine particle motion.

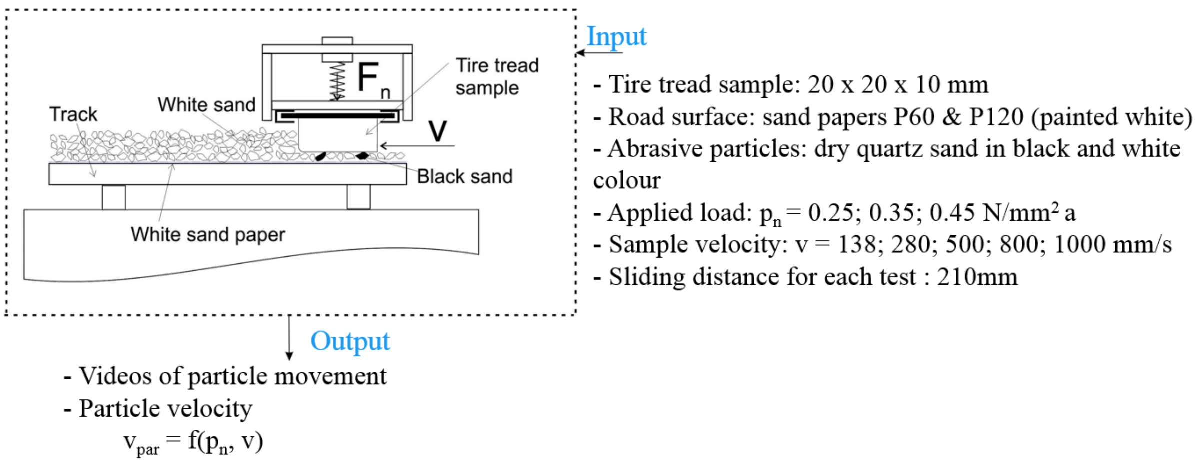

Figure 12. Schematic diagram of the investigation of particle displacements

A high-speed camera serves to record videos of black particles and sample movements, as shown in Figure 13. Image processing is then applied to analyze the record videos and define the velocities of black particles.

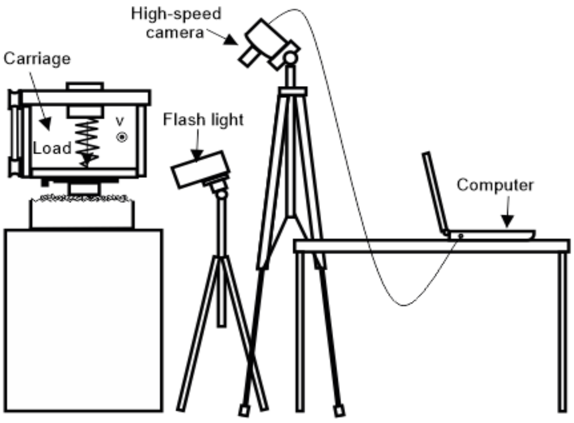

Figure 13. Schematic model of the movement observation tester

The results and approximate curves of experimental data are shown in Figure 14. When sample velocity increases, the particle layer's velocity increases as well and the value of the particle layer's velocity is about half of the sample velocity. However, the particle layer's velocity is almost constant when the normal pressure rises.

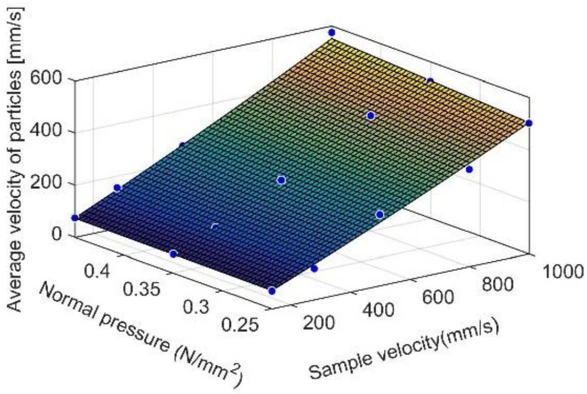

Figure 14. Experimental results and approximiate curve of experimental data of the particles displacement

The surface fitting is used to determine an approximate function v_{par} = f (p_n,v_{sa}) that characterizes the relationship of the particle layer's velocity to normal pressure p_n and sample velocity v_{sa}. The general equation of surface fitting approximation is given as follows

$$v_{par} = p_{00} + p_{10}v_{sa} + p_{01}p_n + p_{20}v_{sa}^2 + p_{11}v_{sa}p_n \tag{15}$$

$p_{i,j}$ are coefficients, given in table 2.

Table 2: Values of coefficients in the surface fitting equation

p_{00}	p_{10}	p_{01}	p_{20}	p_{11}
12.06	0.3848	19.59	$4.76 \cdot 10^{-5}$	0.2561

4 NUMERICAL SIMULATION RESULTS OF THE TIRE TREAD SAMPLE

To carry out the wear simulation of the tire tread sample, besides the geometry and material properties of the tire tread sample, particles, and road surface described above, other input parameters such as normal pressure, velocity of sample, sliding distance, and simulation time are necessary. These parametes are listed in table 3.

Table 3: Input parameters for wear simulation

Input parameters	Range
Normal pressure	p_n = 0.25- 0.45 N/mm^2
Velocity of sample	v_{sa} = 500 mm/s
Sliding distance	SL = 0 - 30 m
Simulation step	ΔX = 10 mm
Time simulation step	Δt = 0.02 s
Length of road	1 m

4.1 Wear mass, wear rate and the worn surface shape

Figure 15 a) shows the relation between the wear mass and the sliding distance at normal pressure p_n = 0.35 N/mm^2 and sample velocity v = 500 mm/s. The dependency of wear mass on the sliding distance is nonlinear. Wear mass increases as the sliding distance increases. The relation of the wear rate and the sliding distance is shown in Figure 15 b). It can be seen that with increased sliding distance the wear rate reduces rapidly during the first 200 mm. This behavior in the run-in phase can be explained by the initial surface roughness and the contact condition which influence parameters governing the wear and which causes significant change of the wear rate in this stage. Afterwards, the wear rate reaches a steady state.

a) b)

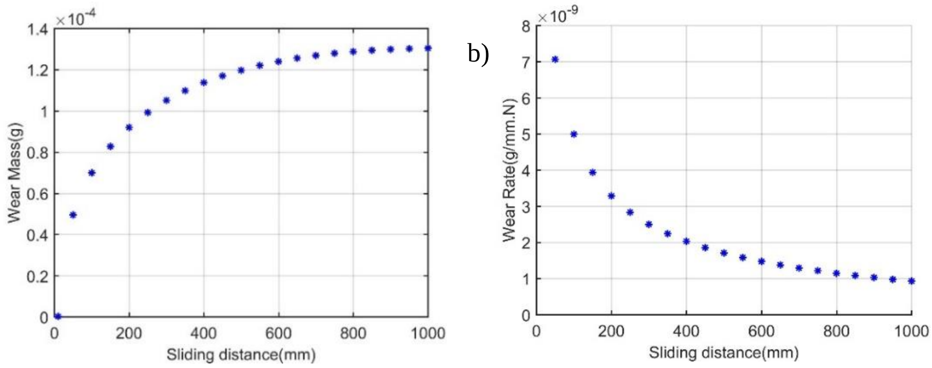

Figure 15. Simulated relation of the sliding distance with wear mass (a) and wear rate (b)

The worn surface shapes of the tire tread sample at different sliding distance are shown in Figure 16 a). The wear of the contact nodes at leading edge are greater than that of the contact nodes at the trailing edge of the tire tread sample. Because of the lifting the road surface, at contact nodes of the trailing edge there are less forces and thus causes less wear. the amount of wear of the contact nodes increases rapidly during the first 500 mm of sliding distance and decreases thereafter.

a) b)

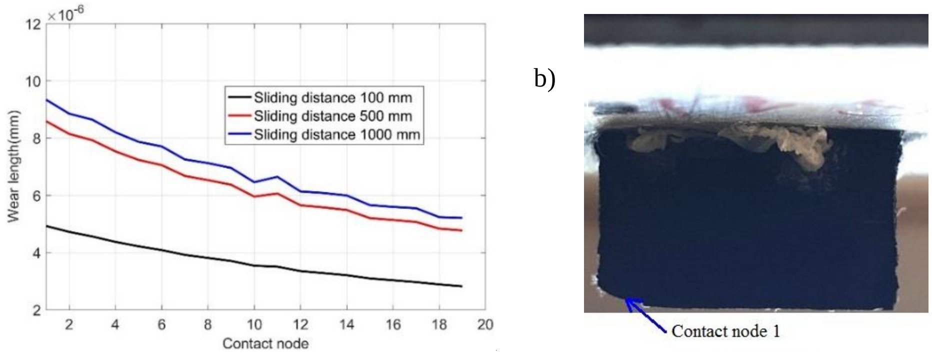

Figure 16. The simulation (a) and real (b) worn surface shapes of the tire tread sample

Figure 17 a) shows the wear rates of the 3 nodes at the inlet, middle, and outlet positions. These nodes are numbered 1, 9, and 19, respectively, as shown in figure 17 b). The wear rate has the largest value at node 1 (inlet node) and the smallest value at node 19 (outlet node). The wear rate of all three contact nodes decrease after 600 mm sliding distance.

a) b)

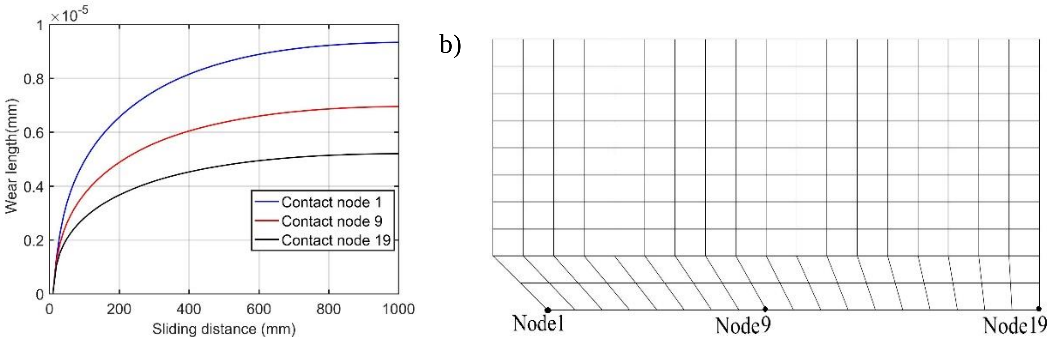

Figure 17. The wear rate of contact nodes (a) and the position of contact nodes (b)

Figure 18 shows the wear mass value of the sample at different normal pressures p_n = 0.25, 0.35, and 0.45 N/mm^2 with the same sample velocity v = 500 mm/s. It can be seen that the relationship of wear mass to the sliding distance is an almost linear relationship. Wear mass increases as the normal pressure increases.

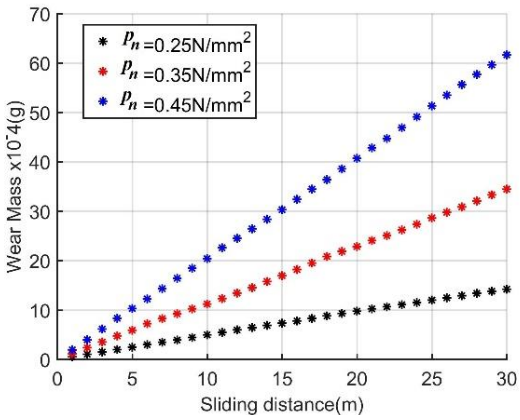

Figure 18. Simulated wear mass of the tire sample at different normal pressures and constant sample velocity

4.2 Comparision with experiments

Within this section, the results of the wear simulation are compared with experimental results. The rubber samples with the same test configuration as p_n = 0.25, 0.35 and 0.45 N/mm^2, sample velocity v = 500 mm/s, and sandpaper 120 plays the role of the road surface. Results of the experimental investigation compared with the wear simulation are displayed in Figure 19 a) and b). It shows a quite good agreement at p_n = 0.25 and 0.35 N/mm^2. However, at p_n = 0.45

N/mm^2, the deviation between experimental and simulation results increases as the sliding distance increases. This is explained by during the experiment at p_n = 0.45 N/mm^2, at some point the sample is not in direct contact with the particles, but in contact with the road surface and causing the wear of the sample to increase.

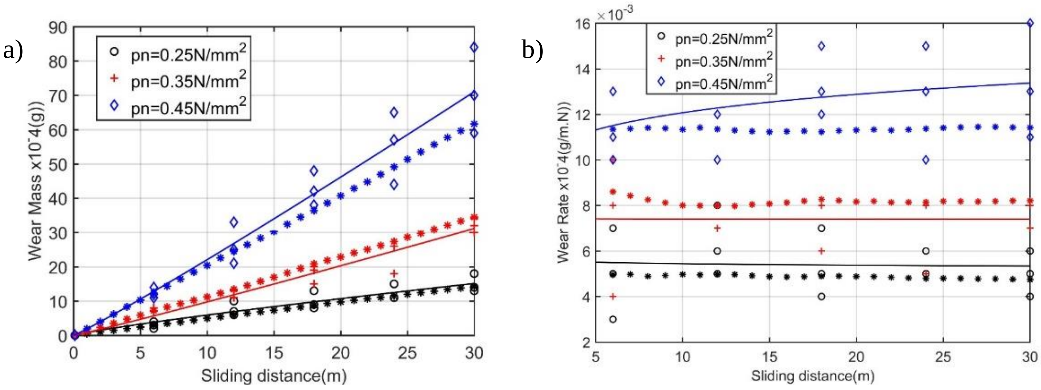

Figure 19. Comparision of the wear mass (a) and wear rate (b) between simulation and experimental results

5 CONCLUSIONS

A numerical simulation using FEM was performed to analyze the wear process of the tire tread sample. The wear process is described by a new three-body wear model which is developed based on physical effects. During the wear simulation, the mass matrix M and stiffness matrix K of the tire tread sample are changed due to the change in geometry of the sample due to wear. In this wear simulation model, some approximation equations representing the friction coefficient, velocity of the particle layer, and the gap between tire sample and road surface are added to the wear equation. The boundary of the model is limited on tested process parameters such as the applied load p_n up to 0.45 N/mm^2, the velocity v up to 1000 mm/s, and the properties of the tested material.

REFERENCES

[1] Fang, L., et al.: *Movement patterns of abrasive particles in three-body abrasion*. In: Wear, 162-164, pp. 782-789, 1993

[2] Fang, L.; Kong, X.L.; Zhou, Q.: *A wear tester capable of monitoring and evaluating the movement pattern of abrasive particles in three-body abrasion*. In: Wear 159, pp. 115-120, 1992

[3] Wu, J., et al.: *Wear predicted model of tread rubber based on experimental and numerical method*. Exp. Tech. 42(2), 191–198 (2018)

[4] Wu, J.; et al.: *Experiment and Simulation Research on the FatigueWear of Aircraft Tire Tread Rubber*. Polymers 2021, 13, 1143

[5] Nikishkow, G.P.: *Introduction to the finite element method*. In: Lecture Notes, University of Aizu, 2004

[6] Kwon, Y.W., Bang, H.: *The Finite Element Method Using MATLAB*, ISBN 0-8493-9653-0, CRC mechanical engineering series, 1997

[7] Manuel Alejandro Tapia-Romero, Mariamne Dehonor-Gómez and Luis Edmundo Lugo-Uribe. *Prony series calculation for viscoelastic behavior modeling of structural adhesives from DMA data*. Ing. invest. y tecnol.. Vol. 21(2)

[8] *Structural Mechanics Module User's Guide*. Version COMSOL 4.3.b, May 2013

[9] Moldenhauer, P.: *Modellierung und Simulation der Dynamik und des Kontakts von Reifenprofilblöcken*. In: Diss.,Technischen Universität Bergakademie Freiberg, 2010

[10] Cho, J. C. ; Jung, C.: *Prediction of Tread PatternWear by an Explicit Finite Element Model*. In: *Tire Science and Technology* 35 (2007), Nr. 4, S. 279–299